isvr Institute of Sound and Vibration Research

Application of the Dynamic Stiffness Method to the Vibration of Helical Springs

J. Lee and D.J. Thompson

ISVR Technical Memorandum 842

August 1999

University of Southampton

SCIENTIFIC PUBLICATIONS BY THE ISVR

Technical Reports are published to promote timely dissemination of research results by ISVR personnel. This medium permits more detailed presentation than is usually acceptable for scientific journals. Responsibility for both the content and any opinions expressed rests entirely with the author(s).

Technical Memoranda are produced to enable the early or preliminary release of information by ISVR personnel where such release is deemed to the appropriate. Information contained in these memoranda may be incomplete, or form part of a continuing programme; this should be borne in mind when using or quoting from these documents.

Contract Reports are produced to record the results of scientific work carried out for sponsors, under contract. The ISVR treats these reports as confidential to sponsors and does not make them available for general circulation. Individual sponsors may, however, authorize subsequent release of the material.

UNIVERSITY OF SOUTHAMPTON

INSTITUTE OF SOUND AND VIBRATION RESEARCH

DYNAMICS GROUP

Application of the Dynamic Stiffness Method to the Vibration of Helical Springs

by

J. Lee and D.J. Thompson

ISVR Technical Memorandum No. 842

August 1999

Authorized for issue by
Dr M.J. Brennan
Group Chairman

ABSTRACT

By using Frenet formulation and Timoshenko beam theory, the partial differential equations of motion are derived for a helical spring having a doubly symmetrical cross section. These are solved to give the relation between wave number and frequency along with the associated wave shapes. From these the dynamic stiffness matrix is assembled. Natural frequencies and related wave numbers are obtained from the receptance of the system. The results of the dynamic stiffness method are compared with those of the transfer matrix method and the finite element method from published examples. Displacements are also found from the dynamic stiffness matrix under a given loading condition. The nature of the wave propagation obtained using the presented method is also investigated.

CONTENTS

NOTATION

A	cross-sectional area of wire
a_i	coefficients of displacement of wire
c_{ph}	phase velocity of the wave
E, G	Young's modulus, shear modulus
F	force vector
f	frequency of oscillation
H	mass and mass moment of inertia matrix
h	axial length of the spring
I_u, I_v, I_w	moments of area about diameter of cross-section
K	Dynamic stiffness matrix
k	wave number
M_u, M_v, M_w	resulting moments in the wire
n	number of active turns
P	applied forces acting on the spring
P_u, P_v, P_w	resulting forces acting on cross-section
Q	transformation matrix of the helical system
R	radius of the helix
r	radius of a wire of circular cross-section
s	distance measured along the helix
$\mathbf{S}_{ij}$	system matrix, Appendix A
T	transformation matrix of a helical spring
t	time
U	displacement vector
(u, v, w)	co-ordinate system measured along the helix of the spring
$\hat{\mathbf{u}}, \hat{\mathbf{v}}, \hat{\mathbf{w}}$	unit vectors of the co-ordinate system (u, v, w)
V	torsional wave in the wire without bending (ref. 4)
V'	bending wave in the wire without torsion (ref. 4)
(x, y, z)	co-ordinate system measured along the axis of the spring
α	helix angle
Δ	magnitude of translational displacement

δ	displacement vector of wire
ϕ	angle measured along the wire
γ	shear coefficient for cross-section
φ	mode shape vector
κ	curvature of helix
Λ	magnitude of rotation
ρ	density of wire material
τ	tortuosity of helix
ν	Poisson's ratio
Π	magnitude of force
Θ	magnitude of moment
$\theta_u, \theta_v, \theta_w$	components of rotation of wire cross section
θ	rotation vector of wire
ω	angular frequency

superscript

-	global coordinate

1. INTRODUCTION

The helical spring is a very common and important element in many machines and vehicles. In dynamic analyses such springs, as well as dampers, are often treated as simple massless force elements. However, as the frequency range of interest increases, such an approach is not suitable for the prediction of the dynamic behaviour of the system. In particular, above a certain frequency, internal resonances of the spring have to be taken into account.

Already a hundred years ago, Love [1] gave the equations of motion for a coil spring. However, these twelfth order differential equations could not be solved analytically. In the 1930s Timoshenko [2] derived the rigidity of the compression, lateral and shear deflections for a coil spring in order to explain the bounds of stability of a compressed helical spring due to lateral buckling.

Axial vibrations of helical springs are described by Wahl [3]. For a circular wire, he showed that the fundamental natural frequency of a spring, clamped at both ends, is given by:

$$f_1 = \frac{r}{8n\pi R^2}\left(\frac{2G}{\rho}\right)^{1/2} \tag{1}$$

where r is the radius of the wire, R is the radius of the helix, n is the number of turns, G is the shear modulus and ρ is the density. Other natural frequencies were integer multiples of f_1.

Wittrick's paper [4] of 1966 is a classic treatise on the behaviour of helical springs. Prior to this, as given by Wahl, in analyses of the propagation of extensional waves along the axis of a helical spring it was assumed that the coupling between extension of the spring and rotation about its axis could be ignored. By including this coupling Wittrick showed that there are two basic wave velocities. One, V, is of a wave involving torsion in the wire with no bending, while the other, V', is of a wave involving bending but no torsion. Both wave velocities were shown to be independent of the helix angle as well as the frequency. They were given as:

$$V = \frac{1}{R}\left(\frac{GI_w}{\rho A}\right)^{1/2} \quad ; \quad V' = \frac{1}{R}\left(\frac{EI_v}{\rho A}\right)^{1/2} \tag{2,3}$$

where A is the cross-sectional area of the wire and EI_v and GI_w are the rigidities for flexure and torsion of the wire about the binormal and axial directions respectively. These velocities are given relative to the distance along the wire. The velocity V corresponds exactly to Wahl's natural frequencies if the wire is circular in cross-section.

These two types of wave were shown by Wittrick to exist independently, but since both involve extension of the spring and rotation about its axis, in general they occur simultaneously.

Wittrick treated the helical spring as a Timoshenko beam including shear deformation and rotational inertia and obtained a set of twelve linear coupled partial differential equations. These were the most complete equations at the time, and apart from minor corrections, have been used by a number of authors since. He obtained approximate solutions in several ways but did not obtain an exact solution.

Jiang *et al.* [5, 6] obtained non-linear equations of motion and from them linearised equations for the vibration of a spring. They studied the coupling between axial and torsional motion in more detail than Wittrick, deriving the complex form of the oscillations of the spring in the time domain due to the interaction and superposition of the component waves.

Sinha and Costello [7] used a finite difference technique and the method of non-linear characteristics to solve numerically the non-linear partial differential equations in the time domain. This study too is limited to axial and torsional motion of the spring.

It is not a simple matter to extend the above analyses to include out of plane motion of the spring. The axial and torsional motions can be likened to those of a simple rod, but coupling between the different equations of motion makes such an analogy less useful for the out-of-plane motion. However, with the aid of digital computers it is possible to solve the differential equations as given by Love or Wittrick.

In a different approach Lee *et al.* [8] used 432 Euler beam finite elements to represent a coil spring having six turns in order to investigate the resonance effect on the vehicle suspension system and body. These were reduced to six super-elements to ease analysis within a vehicle model.

Mottershead [9] developed special finite elements for solving the differential equations. He obtained element displacement functions by integrating the differential equations. The elements so obtained may be one or more turns of the spring in length or a fraction of a turn. For static problems his elements provide exact solutions whilst for dynamics the natural frequencies are unaffected by mesh density provided that sufficient master degrees of

freedom are specified. Mottershead also performed experiments on two small clamped-clamped springs, the results of which have been used by other researchers to test their theories. As well as predominantly extensional and torsional modes, 'snaking' modes that also involve transverse motion were found that can explain the side wear of coils under axial loading. Such modes cannot be detected by using simple theories.

Another approach is the transfer matrix method, employed by Pearson [10]. He obtained the partial differential equations of motion for a helical spring subject to a static axial preload. The transfer matrix was obtained from the differential equations by a series expansion. This series does not converge if the spring is too long, so usually the spring is sub-divided into 2^m equal segments. The natural frequencies were found as the zeroes of the determinant of a 6×6 frequency dependent matrix. An iterative method was used for this. Pearson shows the dependence of the natural frequencies on axial load, helix angle, number of turns etc.

Yildirim [11] also used the transfer matrix approach, making use of the Cayley-Hamilton theorem to develop an algorithm which allows the transfer matrix to be determined with improved precision. This is especially important for long springs. In [12] Yildirim concentrates on determining the natural frequencies for arbitrarily shaped springs. In [13] an efficient method for determining the natural frequencies is developed.

In [14] Pearson and Wittrick used the dynamic stiffness method to find an exact solution for the natural frequencies of a coil spring based on Bernoulli-Euler beam theory and an adaptation of the Wittrick-Williams algorithm. Although efficient and analytically exact, this work does not include shear effects in the wire.

In this report the governing partial differential equations of motion of a helical spring are derived based on Timoshenko beam theory and Frenet's formulation for curved systems (as in [9-11]). From these equations the dispersion relation, linking wave number and frequency for each wave, is studied. By a summation of waves, a frequency-dependent dynamic stiffness matrix, $\mathbf{K}$ is determined that links the six degrees of freedom at each end of the spring to the six forces/moments at each end. After applying suitable constraints, the frequencies at which the determinant of $\mathbf{K}$ vanishes are the natural frequencies of the spring. Moreover the dynamic stiffness matrix can be used as an "exact" element in a model of a more complicated structure, for example a vehicle.

2. THEORETICAL BACKGROUND AND FORMULATION

2.1. Static equilibrium

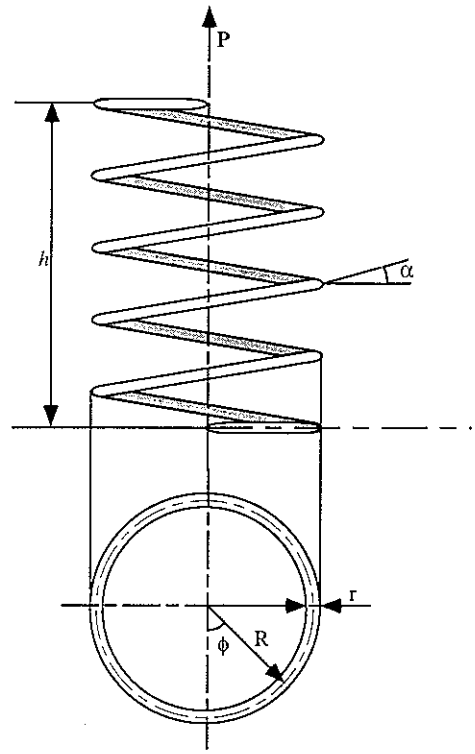

Fig. 1 Statically loaded helical spring

Consider the uniform spring wound from wire, the central axis of which forms a right-handed helix of radius R with helix angle α. The spring is subjected to a static axial load **P**, as shown in Fig. 1. Then at any cross-section the wire is subjected to three components of force P_u, P_v, P_w and three moments M_u, M_v, M_w about the normal $\hat{\mathbf{u}}$, binormal $\hat{\mathbf{v}}$ and tangential directions $\hat{\mathbf{w}}$ (see Fig. 2). These forces and moments result in the linear and rotational displacements of the wire and cause the coupling effects of motion of the spring. It will be assumed that the cross-section of the wire has two axes of symmetry which coincide with the directions $\hat{\mathbf{u}}$ and $\hat{\mathbf{v}}$. At the position s on the spring measured along the wire,

$$\phi = s\cos\alpha / R \tag{4}$$

and

$$x = s\sin\alpha = R\phi\tan\alpha \tag{5.a}$$

$$y = R\cos\phi \tag{5.b}$$

$$z = R\sin\phi \tag{5.c}$$

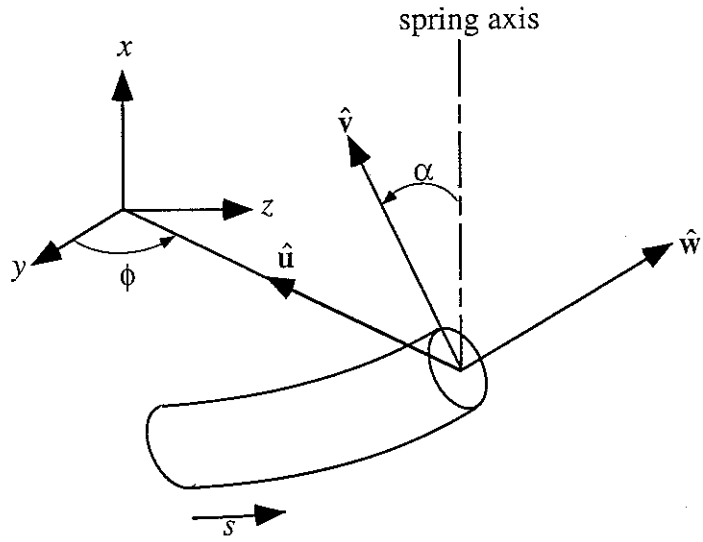

Fig. 2 Coordinate system of a helical spring

The displacements (u, v, w) in local co-ordinates are related to global co-ordinates (x, y, z) by

$$\begin{Bmatrix} u \\ v \\ w \end{Bmatrix} = \begin{bmatrix} 1 & 0 & 0 \\ 0 & \cos\alpha & -\sin\alpha \\ 0 & \sin\alpha & \cos\alpha \end{bmatrix} \begin{bmatrix} 0 & -\cos\phi & -\sin\phi \\ 1 & 0 & 0 \\ 0 & -\sin\phi & \cos\phi \end{bmatrix} \begin{Bmatrix} u_x \\ u_y \\ u_z \end{Bmatrix}$$
$$= \begin{bmatrix} 0 & -\cos\phi & -\sin\phi \\ \cos\alpha & \sin\alpha\sin\phi & -\sin\alpha\cos\phi \\ \sin\alpha & -\cos\alpha\sin\phi & \cos\alpha\cos\phi \end{bmatrix} \begin{Bmatrix} u_x \\ u_y \\ u_z \end{Bmatrix} = [\mathbf{Q}] \begin{Bmatrix} u_x \\ u_y \\ u_z \end{Bmatrix} \tag{6}$$

Similar equations apply for rotations, forces and moments.

Frenet formulation [15] allows all of the displacements and resultant forces to be given as functions of s, the measured length along the helix from one end of the helical spring as shown in Fig. 2. The curvature κ and tortuosity τ of the helix are defined by

$$\kappa = \frac{\cos^2\alpha}{R} \tag{7}$$

$$\tau = \frac{\sin\alpha\cos\alpha}{R} \tag{8}$$

The relations between these parameters and the three unit vectors are [15]

$$\frac{\partial}{\partial s}\begin{Bmatrix}\hat{\mathbf{u}}\\ \hat{\mathbf{v}}\\ \hat{\mathbf{w}}\end{Bmatrix}=\begin{bmatrix}0 & \tau & -\kappa\\ -\tau & 0 & 0\\ \kappa & 0 & 0\end{bmatrix}\begin{Bmatrix}\hat{\mathbf{u}}\\ \hat{\mathbf{v}}\\ \hat{\mathbf{w}}\end{Bmatrix} \tag{9}$$

Suppose the components of the linear displacements $\boldsymbol{\delta}$, rotations $\boldsymbol{\theta}$, concentrated forces $\mathbf{P}$ and moments $\mathbf{M}$ at position s are defined by

$$\begin{Bmatrix}\boldsymbol{\delta}\\ \boldsymbol{\theta}\\ \mathbf{P}\\ \mathbf{M}\end{Bmatrix}=\begin{bmatrix}\delta_u & \delta_v & \delta_w\\ \theta_u & \theta_v & \theta_w\\ P_u & P_v & P_w\\ M_u & M_v & M_w\end{bmatrix}\begin{Bmatrix}\hat{\mathbf{u}}\\ \hat{\mathbf{v}}\\ \hat{\mathbf{w}}\end{Bmatrix} \tag{10}$$

Differentiating equation (10) by the length measured along the helix s,

$$\frac{d}{ds}\begin{Bmatrix}\boldsymbol{\delta}\\ \boldsymbol{\theta}\\ \mathbf{P}\\ \mathbf{M}\end{Bmatrix}=\left(\frac{\partial}{\partial s}\begin{bmatrix}\delta_u & \delta_v & \delta_w\\ \theta_u & \theta_v & \theta_w\\ P_u & P_v & P_w\\ M_u & M_v & M_w\end{bmatrix}\right)\begin{Bmatrix}\hat{\mathbf{u}}\\ \hat{\mathbf{v}}\\ \hat{\mathbf{w}}\end{Bmatrix}+\begin{bmatrix}\delta_u & \delta_v & \delta_w\\ \theta_u & \theta_v & \theta_w\\ P_u & P_v & P_w\\ M_u & M_v & M_w\end{bmatrix}\left(\frac{\partial}{\partial s}\begin{Bmatrix}\hat{\mathbf{u}}\\ \hat{\mathbf{v}}\\ \hat{\mathbf{w}}\end{Bmatrix}\right) \tag{11}$$

Substitute equations (9) into the second term of right hand side of equation (11) and rearrange to give

$$\frac{d}{ds}\begin{Bmatrix}\boldsymbol{\delta}\\ \boldsymbol{\theta}\\ \mathbf{P}\\ \mathbf{M}\end{Bmatrix}=\begin{bmatrix}\frac{\partial\delta_u}{\partial s}-\tau\delta_v+\kappa\delta_w & \frac{\partial\delta_v}{\partial s}+\tau\delta_u & \frac{\partial\delta_w}{\partial s}-\kappa\delta_u\\ \frac{\partial\theta_u}{\partial s}-\tau\theta_v+\kappa\theta_w & \frac{\partial\theta_v}{\partial s}+\tau\theta_u & \frac{\partial\theta_w}{\partial s}-\kappa\theta_u\\ \frac{\partial P_u}{\partial s}-\tau P_v+\kappa P_w & \frac{\partial P_v}{\partial s}+\tau P_u & \frac{\partial P_w}{\partial s}-\kappa P_u\\ \frac{\partial M_u}{\partial s}-\tau M_v+\kappa M_w & \frac{\partial M_v}{\partial s}+\tau M_u & \frac{\partial M_w}{\partial s}-\kappa M_u\end{bmatrix}\begin{Bmatrix}\hat{\mathbf{u}}\\ \hat{\mathbf{v}}\\ \hat{\mathbf{w}}\end{Bmatrix} \tag{12}$$

Timoshenko beam theory [2] gives the relationship between displacements and forces as

$$\frac{d}{ds}\begin{Bmatrix}\boldsymbol{\delta}\\ \boldsymbol{\theta}\\ \mathbf{P}\\ \mathbf{M}\end{Bmatrix}=\begin{bmatrix}\frac{P_u}{GA\gamma}+\theta_v & \frac{P_v}{GA\gamma}-\theta_u & \frac{P_w}{EA}\\ \frac{M_u}{EI_u} & \frac{M_v}{EI_v} & \frac{M_w}{GI_w}\\ 0 & 0 & 0\\ P_v & -P_u & 0\end{bmatrix}\begin{Bmatrix}\hat{\mathbf{u}}\\ \hat{\mathbf{v}}\\ \hat{\mathbf{w}}\end{Bmatrix} \tag{13}$$

Substituting equation (13) into equation (12), the governing partial differential equations for the static equilibrium are obtained as follows

$$\frac{\partial}{\partial s}\begin{Bmatrix}\boldsymbol{\delta}\\ \boldsymbol{\theta}\\ \mathbf{P}\\ \mathbf{M}\end{Bmatrix}=\begin{bmatrix}\frac{P_u}{GA\gamma}+\theta_v+\tau\delta_v-\kappa\delta_w & \frac{P_v}{GA\gamma}-\theta_u-\tau\delta_u & \frac{P_w}{EA}+\kappa\delta_u\\ \frac{M_u}{EI_u}+\tau\theta_v-\kappa\theta_w & \frac{M_v}{EI_v}-\tau\theta_u & \frac{M_w}{GI_w}+\kappa\theta_u\\ \tau P_v-\kappa P_w & -\tau P_u & \kappa P_u\\ P_v+\tau M_v-\kappa M_w & -P_u-\tau M_u & \kappa M_u\end{bmatrix}\begin{Bmatrix}\hat{\mathbf{u}}\\ \hat{\mathbf{v}}\\ \hat{\mathbf{w}}\end{Bmatrix} \tag{14}$$

Rearranging by components of displacements and forces,

$$\frac{\partial}{\partial s}\begin{Bmatrix}\boldsymbol{\delta}\\ \boldsymbol{\theta}\\ \mathbf{P}\\ \mathbf{M}\end{Bmatrix}=\begin{bmatrix}\mathbf{S}_{11} & \mathbf{S}_{12}\\ \mathbf{0} & \mathbf{S}_{22}\end{bmatrix}\begin{Bmatrix}\boldsymbol{\delta}\\ \boldsymbol{\theta}\\ \mathbf{P}\\ \mathbf{M}\end{Bmatrix} \tag{15}$$

where $\mathbf{S}_{ij}$ is the system matrix defined in Appendix A. Note that $\mathbf{S}_{12}$ is diagonal, whereas $\mathbf{S}_{11}=\mathbf{S}_{22}^{T}$ are not symmetric.

2.2. Dynamic equilibrium

In the D'Alembert view of dynamic equilibrium of equation (15), inertia forces are considered to act in opposition to elastic forces. Introducing the inertia forces into equation (15), the governing partial differential equations for the dynamic equilibrium are equation (16) that is essentially the same as Wittrick's governing differential equation [4].

$$\frac{\partial}{\partial s}\begin{Bmatrix}\boldsymbol{\delta}\\ \boldsymbol{\theta}\\ \mathbf{P}\\ \mathbf{M}\end{Bmatrix}=\begin{bmatrix}\mathbf{S}_{11} & \mathbf{S}_{12}\\ \mathbf{0} & \mathbf{S}_{22}\end{bmatrix}\begin{Bmatrix}\boldsymbol{\delta}\\ \boldsymbol{\theta}\\ \mathbf{P}\\ \mathbf{M}\end{Bmatrix}+\begin{bmatrix}\mathbf{0} & \mathbf{0}\\ \mathbf{T}_{21} & \mathbf{0}\end{bmatrix}\frac{\partial^2}{\partial t^2}\begin{Bmatrix}\boldsymbol{\delta}\\ \boldsymbol{\theta}\\ \mathbf{P}\\ \mathbf{M}\end{Bmatrix} \tag{16}$$

where $\mathbf{T}_{ij}$ is the inertia force matrix defined in Appendix A. Note that $\mathbf{T}_{21}$ is diagonal. Equation (16) describes the dynamic behaviour of a helical spring.

2.3. Dispersion relationship

A wave in the spring is composed of temporal and spatial variation. The temporal variation is characterised by the angular frequency ω and the spatial variation is characterised by the wave number k. The form of relationship between wave number k and angular frequency ω is termed the dispersion relationship as follows.

$$\mathrm{k}=\frac{j\omega}{c_{ph}} \tag{17}$$

where c_{ph} represents the phase velocity of the wave.

The translational and the rotational motions and the stress for an element of the wire all have the same spatial dependence so if the responses of an element of the wire are harmonic in time, we write the displacements and forces for a particular free wave as

$$\begin{Bmatrix}\boldsymbol{\delta}\\ \boldsymbol{\theta}\\ \mathbf{P}\\ \mathbf{M}\end{Bmatrix}=\begin{Bmatrix}\Delta\\ \Theta\\ \Pi\\ \Lambda\end{Bmatrix}e^{ks+j\omega t} \tag{18}$$

Substitution of equation (18) into equation (16) gives the set of twelve homogeneous linear simultaneous equations.

$$k\begin{Bmatrix}\Delta\\ \Theta\\ \Pi\\ \Lambda\end{Bmatrix}=\left(\begin{bmatrix}\mathbf{S}_{11} & \mathbf{S}_{12}\\ \mathbf{0} & \mathbf{S}_{22}\end{bmatrix}-\omega^2\begin{bmatrix}\mathbf{0} & \mathbf{0}\\ \mathbf{T}_{21} & \mathbf{0}\end{bmatrix}\right)\begin{Bmatrix}\Delta\\ \Theta\\ \Pi\\ \Lambda\end{Bmatrix} \tag{19}$$

Rewrite equation (19),

$$\left(k[\mathbf{I}]-\begin{bmatrix}\mathbf{S}_{11} & \mathbf{S}_{12}\\ \mathbf{S}_{21}^{*} & \mathbf{S}_{22}\end{bmatrix}\right)\begin{Bmatrix}\Delta\\ \Theta\\ \Pi\\ \Lambda\end{Bmatrix}=\mathbf{0} \tag{20}$$

where $\mathbf{S}_{21}^{*}=-\omega^2\mathbf{T}_{21}$. In order that equation (20) should have a non-zero solution, it is necessary for the determinant to vanish, thus

$$\det\left|k[\mathbf{I}]-\begin{bmatrix}\mathbf{S}_{11} & \mathbf{S}_{12}\\ \mathbf{S}_{21}^{*} & \mathbf{S}_{22}\end{bmatrix}\right|=0 \tag{21}$$

This is an ordinary eigenvalue problem of dimension 12. It follows that there are twelve wave numbers, six relating to the forward direction and six to backward direction velocities of wave propagation. If the frequency is given, the free wave numbers can be found from the eigen solutions of the system matrix of equation (20). The eigenvectors $\{\Delta\ \Theta\ \Pi\ \Lambda\}^T$ represent the deformation and stresses associated with free wave propagation at wave number k and frequency ω.

2.4. Dynamic stiffness matrix

In this section, the dynamic stiffness matrices are derived for the helical spring system. The relations between loads and displacements are obtained from the first six rows of equation (16).

$$\frac{\partial}{\partial s}\begin{Bmatrix}\delta\\ \theta\end{Bmatrix}=[\mathbf{S}_{11}]\begin{Bmatrix}\delta\\ \theta\end{Bmatrix}+[\mathbf{S}_{12}]\begin{Bmatrix}\mathbf{P}\\ \mathbf{M}\end{Bmatrix} \tag{22}$$

which can be rewritten as

$$\begin{Bmatrix}\mathbf{P}\\ \mathbf{M}\end{Bmatrix} = -[\mathbf{S}_{12}]^{-1}[\mathbf{S}_{11}]\begin{Bmatrix}\delta\\ \theta\end{Bmatrix} + [\mathbf{S}_{12}]^{-1}\frac{\partial}{\partial s}\begin{Bmatrix}\delta\\ \theta\end{Bmatrix} \tag{23}$$

Write the solution as a sum of 12 waves

$$\begin{Bmatrix}\delta\\ \theta\end{Bmatrix} = \sum_{i=1}^{12} a_i\{\varphi_i\}e^{\mathrm{k}_i s}e^{j\omega t} = [\Phi]diag\left(e^{\mathrm{k}_i s}\right)\{a_i\}e^{j\omega t} \tag{24}$$

where $[\Phi]$ is the 6×12 eigenvector matrix associated with equation (21) and a_i are the complex amplitudes of the 12 waves. Differentiate equation (24) with respect to s

$$\frac{\partial}{\partial s}\begin{Bmatrix}\delta\\ \theta\end{Bmatrix} = [\Phi]diag\left(\mathrm{k}_i e^{\mathrm{k}_i s}\right)\{a_i\}e^{j\omega t} \tag{25}$$

Substituting equations (24) and (25) into (23) we obtain for the forces and moments

$$\begin{Bmatrix}\mathbf{P}\\ \mathbf{M}\end{Bmatrix} = -[\mathbf{S}_{12}]^{-1}[\mathbf{S}_{11}][\Phi]diag\left(e^{\mathrm{k}_i s}\right)\{a_i\} + [\mathbf{S}_{12}]^{-1}[\Phi]diag\left(\mathrm{k}_i e^{\mathrm{k}_i s}\right)\{a_i\} \tag{26}$$

Now form the 12×1 vector $\mathbf{U}$ of displacements at $s = 0$ and L from equation (24):

$$\mathbf{U} = \begin{Bmatrix}\delta(0)\\ \theta(0)\\ \delta(L)\\ \theta(L)\end{Bmatrix} = \begin{bmatrix}[\Phi]\\ [\Phi]diag\left(e^{\mathrm{k}_i L}\right)\end{bmatrix}\{a_i\} = \mathbf{D}_1\mathbf{a} \tag{27}$$

and the 12×1 vector $\mathbf{F}$ of forces and moments at $s = 0$ and L from equation (26):

$$\mathbf{F} = \begin{Bmatrix}\mathbf{P}(0)\\ \mathbf{M}(0)\\ \mathbf{P}(L)\\ \mathbf{M}(L)\end{Bmatrix} = \begin{bmatrix}\left(-[S_{12}]^{-1}[S_{11}][\Phi] + [S_{12}]^{-1}[\Phi]diag(\mathrm{k}_i)\right)\\ \left(-[S_{12}]^{-1}[S_{11}][\Phi]diag(e^{\mathrm{k}_i L}) + [S_{12}]^{-1}[\Phi]diag(\mathrm{k}_i e^{\mathrm{k}_i L})\right)\end{bmatrix}\{a_i\} = \mathbf{D}_2\mathbf{a} \tag{28}$$

where $\mathbf{D}_1$ and $\mathbf{D}_2$ are 12×12 matrices. Eliminating **a** from these equations, the dynamic stiffness matrix **K** is given by

$$\mathbf{F} = \mathbf{KU} = \left(\mathbf{D}_2\mathbf{D}_1^{-1}\right)\mathbf{U} \tag{29}$$

To use this it is necessary to convert from local coordinates (u, v, w) to global coordinates (x, y, z), apply boundary conditions and solve. Write a 12×12 matrix

$$\mathbf{T} = \begin{bmatrix} \mathbf{Q}(0) & \mathbf{0} & \mathbf{0} & \mathbf{0} \\ \mathbf{0} & \mathbf{Q}(0) & \mathbf{0} & \mathbf{0} \\ \mathbf{0} & \mathbf{0} & \mathbf{Q}(2n\pi) & \mathbf{0} \\ \mathbf{0} & \mathbf{0} & \mathbf{0} & \mathbf{Q}(2n\pi) \end{bmatrix}^{-1} \tag{30}$$

where $\mathbf{Q}(\phi)$ is the 3×3 rotation matrix given in 2.1. Then if $\overline{\mathbf{F}}$ is force vector at the two ends in (x, y, z) coordinates and $\overline{\mathbf{U}}$ is corresponding displacement vector

$$\overline{\mathbf{F}} = \mathbf{TF} \tag{31}$$

$$\overline{\mathbf{U}} = \mathbf{TU} \tag{32}$$

Then
$$\overline{\mathbf{F}} = \mathbf{TF} = \mathbf{TD}_2\mathbf{D}_1^{-1}\mathbf{U} = \mathbf{TD}_2\mathbf{D}_1^{-1}\mathbf{T}^{-1}\overline{\mathbf{U}} \tag{33}$$

i.e., in global coordinates the dynamic stiffness matrix is

$$\overline{\mathbf{K}} = \mathbf{TD}_2\mathbf{D}_1^{-1}\mathbf{T}^{-1} \tag{34}$$

2.5. Solution for forced response

Suppose the boundary conditions are that for coordinates m the force is known and the displacement unknown and for coordinates l the displacement is known and the force unknown. Then partition $\overline{\mathbf{K}}$

$$\begin{Bmatrix} \overline{\mathbf{F}}_m \\ \overline{\mathbf{F}}_l \end{Bmatrix} = \begin{bmatrix} \overline{\mathbf{K}}_{mm} & \overline{\mathbf{K}}_{ml} \\ \overline{\mathbf{K}}_{lm} & \overline{\mathbf{K}}_{ll} \end{bmatrix} \begin{Bmatrix} \overline{\mathbf{U}}_m \\ \overline{\mathbf{U}}_l \end{Bmatrix} \tag{35}$$

Then taking the upper part and rearranging gives $\overline{\mathbf{U}}_m$ in terms of known quantities

$$\overline{\mathbf{U}}_m = \overline{\mathbf{K}}_{mm}^{-1}\left\{\overline{\mathbf{F}}_m - \overline{\mathbf{K}}_{ml}\overline{\mathbf{U}}_l\right\} \tag{36}$$

Substitute this in the lower part to give

$$\overline{\mathbf{F}}_l = \overline{\mathbf{K}}_{lm}\overline{\mathbf{U}}_m + \overline{\mathbf{K}}_{ll}\overline{\mathbf{U}}_l \tag{37}$$

2.6. Solution for determining resonances

In order to determine the resonances of a spring under specified boundary conditions, maxima are sought in the function

$$\beta = \det\left|\mathbf{K}^{-1}\right| \tag{38}$$

For free-free boundary conditions the full matrix $\mathbf{K}$ is used. For other boundary conditions this has to be reduced. For example, for a spring which is clamped at one end and free at the other, co-ordinates l correspond to the clamped end ($\overline{\mathbf{U}}_l = \{\mathbf{0}\}$). Since the stiffness matrix $\overline{\mathbf{K}}_{ll}$ and coupling stiffness matrices $\overline{\mathbf{K}}_{ml}$, $\overline{\mathbf{K}}_{lm}$ do not affect the co-ordinates m any more, only 6×6 matrix $\overline{\mathbf{K}}_{mm}$ remains.

For a clamped-clamped boundary condition, when the same method is applied, the rank of the stiffness matrix becomes zero. In this case therefore the spring is divided into two substructures at an arbitrary location. These substructures may be analysed by the continuity conditions and the equilibrium equations at the joint. The dynamic stiffness matrix of the whole spring system is derived by assembling the 12×12 dynamic stiffness matrix of each substructure. The assembled dynamic stiffness matrix is

$$\overline{\mathbf{K}} = \begin{bmatrix} \overline{\mathbf{K}}_{mm}^{1} & \overline{\mathbf{K}}_{ml}^{1} & \mathbf{0} \\ \overline{\mathbf{K}}_{lm}^{1} & \overline{\mathbf{K}}_{ll}^{1} + \overline{\mathbf{K}}_{mm}^{2} & \overline{\mathbf{K}}_{ml}^{2} \\ 0 & \overline{\mathbf{K}}_{lm}^{2} & \overline{\mathbf{K}}_{ll}^{2} \end{bmatrix} \tag{39}$$

where the superscript represents the substructure identification. Applying boundary conditions, the dynamic stiffness matrix of the spring is

$$\overline{\mathbf{K}} = \overline{\mathbf{K}}^{1}_{ll} + \overline{\mathbf{K}}^{2}_{mm} \tag{40}$$

Although this may be derived by the continuity conditions and the equilibrium equations at the joint, one must be careful and the process is considerably tedious.

3. EXAMPLES AND DISCUSSION

3.1. Natural frequencies and forced responses

In this section numerical results for three springs are shown and compared with published results. Measurements and predictions for spring 1 and spring 2 have been published by Mottershead [9] and used by Pearson and Yildirim to verify their work [10-13].

Details of each spring are given in Table 1. Since Mottershead [9] does not give material properties of spring 1 and 2, the calculations were performed by using the data of spring 1 given by Yildirim [11] shown in Table 1. Spring 3 is a part of the front suspension of a mid-size passenger car studied by Lee [8].

A finite element model of spring 1 and spring 2 has been assembled using NASTRAN, composed of 350 two node simple beam elements (CBAR) each covering 8 degrees of arc. Spring 3 has been modelled by 432 two-node simple beam each covering 5 degrees of arc. Natural frequencies are obtained by the Lancoz method.

Pearson calculated the overall transfer matrix of the spring which has been divided into six equal segments [10]. By using sequential matrix multiplication, the overall transfer matrix was calculated. Yildirim computed the overall transfer matrix using an algorithm based on the Cayley-Hamilton theorem [11]. The dynamic stiffness method, presented in this report, programmed using MATLAB (see Appendix C), has run on a PC with 300 MHz CPU clock speed. It took about 200 seconds to find the dynamic stiffness matrix and dispersion curve from 1 Hz to 1 kHz with 0.1 Hz frequency resolution.

Natural frequencies are found from the peaks of the determinant of the inverse of the dynamic stiffness matrix (See section 2.6). This function is shown for spring 1 with various boundary conditions in Fig. 3. Natural frequencies for spring 1 and spring 2 with both ends

clamped are compared, in Table 2 and Table 3 respectively, with previously published results. A dash indicates omission of a value. The results of the present finite element analysis are rather different from those obtained by Mottershead [9]. The NASTRAN results are lower than the experimental results by on average 2% whereas Mottershead's results are larger by a similar amount. An important difference between NASTRAN and Mottershead's results are due to not using same material properties although the type of element is also quite different. Differences in material properties probably also have an effect on the calculated results of spring 2 for which Mottershead's results are quite different from the others as shown in Table 3. In this case, the results of current method and the NASTRAN finite element model are in good agreement. Under the transfer matrix method the figure in parenthesis is as shown in Pearson's paper [10], whereas the other figure has been recomputed using parameter values as in Table 1. Comparing the results between Pearson's and Yildirim's method there is little difference except computing time to determine the overall transfer matrix. In general Pearson's method is quicker than Yildirim's.

There is good agreement among the three numerical analysis methods and the experimental results. Especially the dynamic stiffness method presented in this paper is quite accurate for higher modes. Among the numerical analysis methods using the same material and section properties, the dynamic stiffness method gives results which are closer to NASTRAN than the transfer matrix methods.

The variation of the natural frequencies of each spring with changes in boundary conditions is given Tables 4, 5 and 6. Most results show good agreement. However the results from NASTRAN have a lot of discrepancies from the other methods for the case of spring 1 with both ends simply supported.

In the case of the dynamic stiffness method, the forced responses are obtained by equation (36). The forced responses at the resonance frequency are illustrated for spring 1 subjected to an axial force at one end and clamped at another end in Fig. 4. Note that these are not necessarily the free mode shapes.

Table 1. Parameters of helical springs studied

parameters	spring 1	spring 2	spring 3
Coil radius (m)	5×10^{-4}	5×10^{-4}	5×10^{-3}
Helix radius (m)	5×10^{-3}	5×10^{-3}	6.5×10^{-2}
Helix angle (degree)	8.5744	9.78	7.67
No. of active turns	7.6	6	6
Mass density (kg/m^3)	7.9×10^{3}	7.9×10^{3}	8.76×10^{3}
Young's modulus (N/m^2)	2.06×10^{11}	2.06×10^{11}	2.09×10^{11}
Poisson's ratio	0.3	0.3	0.28

Table 2. Comparison of the natural frequencies for spring 1 with both ends clamped. (NAST: NASTRAN, DSM: present method)

	Test	Finite element method	Transfer matrix method				Dynamic stiffness method
(Hz)	Ref. [9]	Ref. [9]	NAST	Ref. [10]		Ref. [11]	DSM
f_1	391	396	383.8	393.4	(394.9)	393.5	388
f_2	391	397	387.1	396.0	(397.6)	395.9	389
f_3	469	459	457.6	462.8	(456.4)	462.8	462
f_4	532	528	513.8	525.6	(518.3)	525.5	526
f_5	878	887	841.7	863.6	(859.7)	864.0	840
f_6	878	900	854.7	876.8	(874.7)	876.9	861
f_7	906	937	911.3	913.6	(902.2)	914.3	926
f_8	-	1067	1011.7	-	(1024.0)	1037.0	1035
f_9	1282	1348	1276.3	-	(1293.0)	1310.5	1265

Table 3. Comparison of the natural frequencies for spring 2 with both ends clamped. (NAST: NASTRAN, DSM: present method)

	Test	Finite element method		Transfer matrix method	Dynamic stiffness method
(Hz)	Ref. [9]	Ref. [9]	NAST	Ref. [10]	DSM
f_1	431	436	467	453	466
f_2	474	478	481	489	480
f_3	490	497	484	526	482
f_4	509	506	569	541	568
f_5	844	856	902	896	900
f_6	932	937	963	977	951
f_7	960	964	985	1032	982
f_8	-	987	1083	1047	1081

Table 4. Natural frequencies of spring 1 with various boundary conditions (BC1: clamped-clamped, BC2: simply supported-simply supported, BC3: clamped-free)

	BC1			BC2			BC3		
(Hz)	NAST	Ref. [11]	DSM	NAST	Ref. [11]	DSM	NAST	Ref. [11]	DSM
f_1	384	394	388	202	203	202	72.1	73.6	73.5
f_2	387	396	389	*203*	*276*	*274*	72.5	73.9	73.9
f_3	458	463	462	381	329	328	226.7	230.7	230.7
f_4	513	526	526	408	448	446	258.1	263.3	263.3
f_5	843	864	864	643	665	663	372.8	380.7	380.7
f_6	856	877	877	655	740	739	374.7	384.2	384.2
f_7	913	914	914	847	-	831	671.4	-	681.0
f_8	1011	1037	1037	890	-	906	761.9	-	773.8

Table 5. Natural frequencies of spring 2 with various boundary conditions using dynamic stiffness method (BC1: clamped-clamped, BC2: simply supported-simply supported, BC3: clamped-free)

(Hz)	BC1	BC2	BC3
f_1	466.1	220.3	100.6
f_2	480.1	331.3	244.1
f_3	482.2	400.3	275.6
f_4	568.1	493.3	459.4
f_5	900.0	706.2	714.9
f_6	951.0	803.7	811.1
f_7	982.4	914.7	965.1
f_8	1081.4	991.2	1038.6

Table 6. Natural frequencies of spring 3 with various boundary conditions (BC1: clamped-clamped, BC2: simply supported-simply supported, BC3: clamped-free)

	BC1			BC2		BC3	
(Hz)	NAST	Ref. [11]	DSM	NAST	DSM	NAST	DSM
f_1	33.06	31.94	32.93	14.14	15.19	7.32	7.19
f_2	34.11	34.90	33.70	24.34	23.31	16.91	16.69
f_3	34.39	36.32	34.18	27.88	28.44	19.11	18.94
f_4	38.99	37.36	38.74	36.67	34.19	32.97	32.69
f_5	64.03	63.55	63.78	45.16	48.69	33.51	33.19
f_6	68.11	69.48	67.78	60.25	56.44	49.94	49.56
f_7	69.90	71.81	69.03	63.47	65.31	56.28	55.81

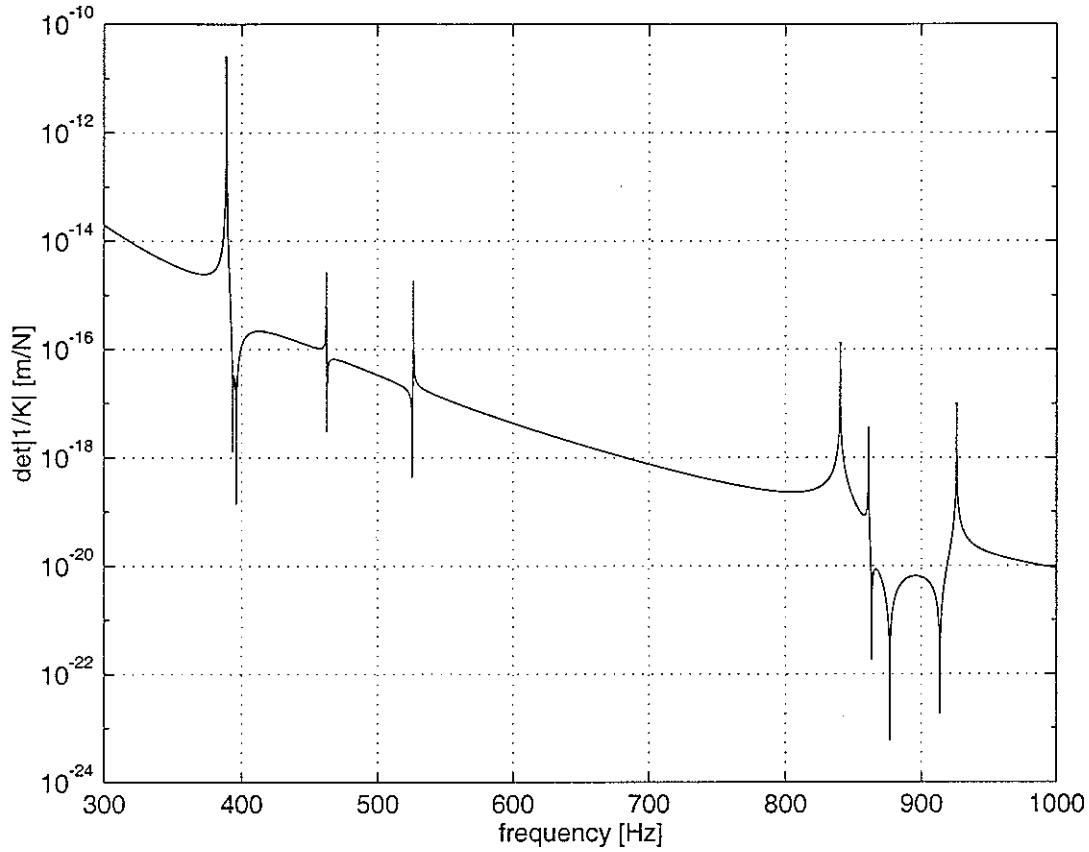

(a) both ends clamped

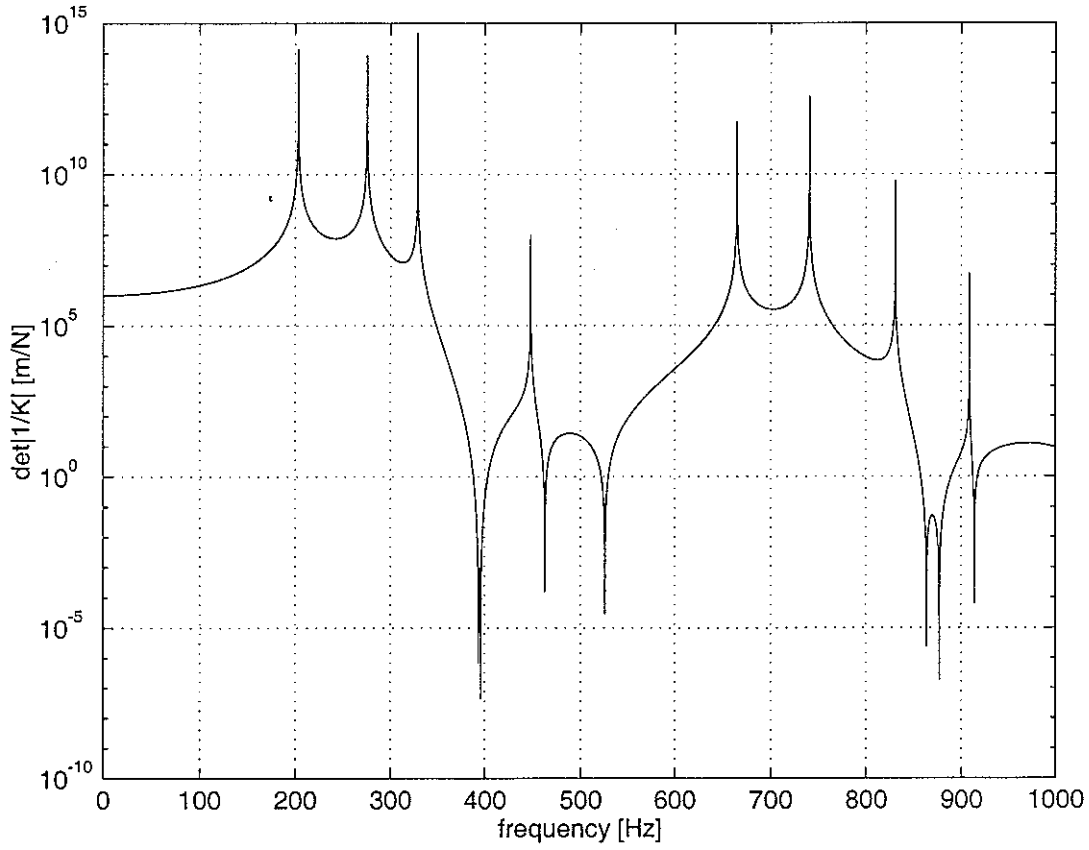

(b) both ends simply supported

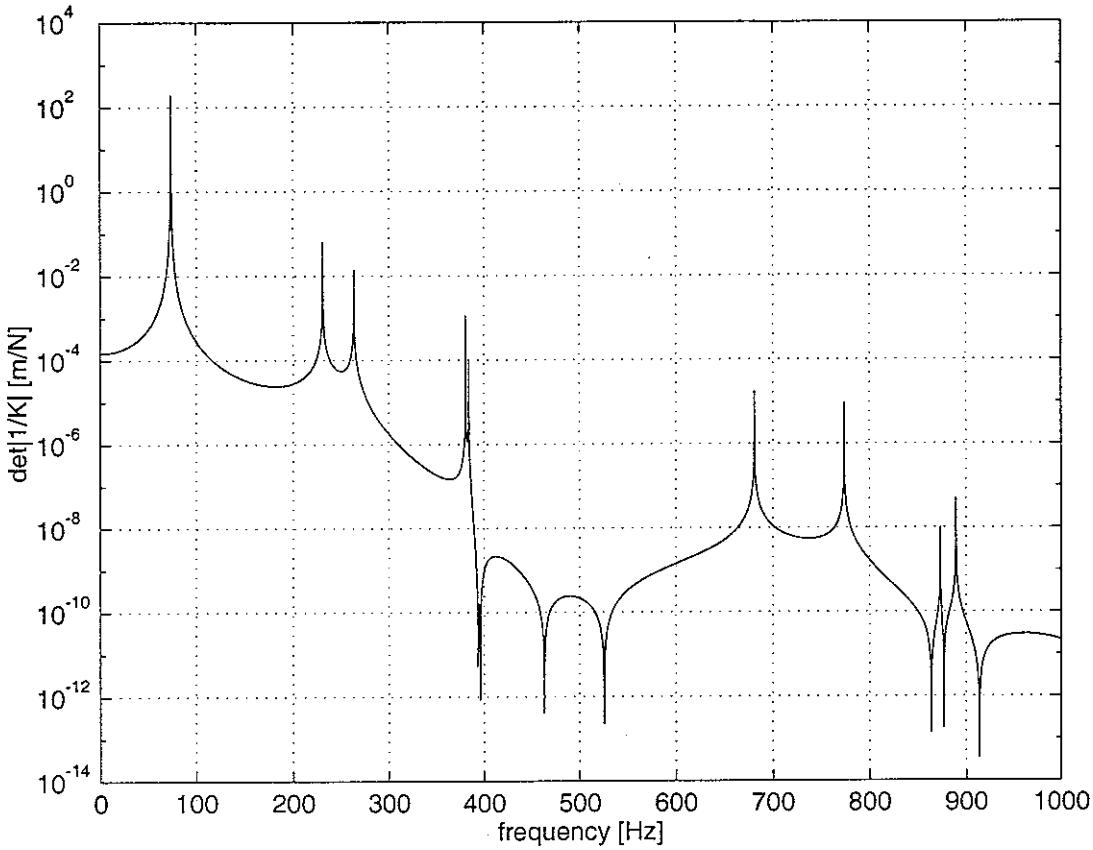

(c) one end clamped the other end free

Fig. 3. $\det\left|\mathbf{K}^{-1}\right|$ of spring 1 calculated by using dynamic stiffness method (a): both ends clamped, (b) both ends simply supported, (c) one end clamped the other end free

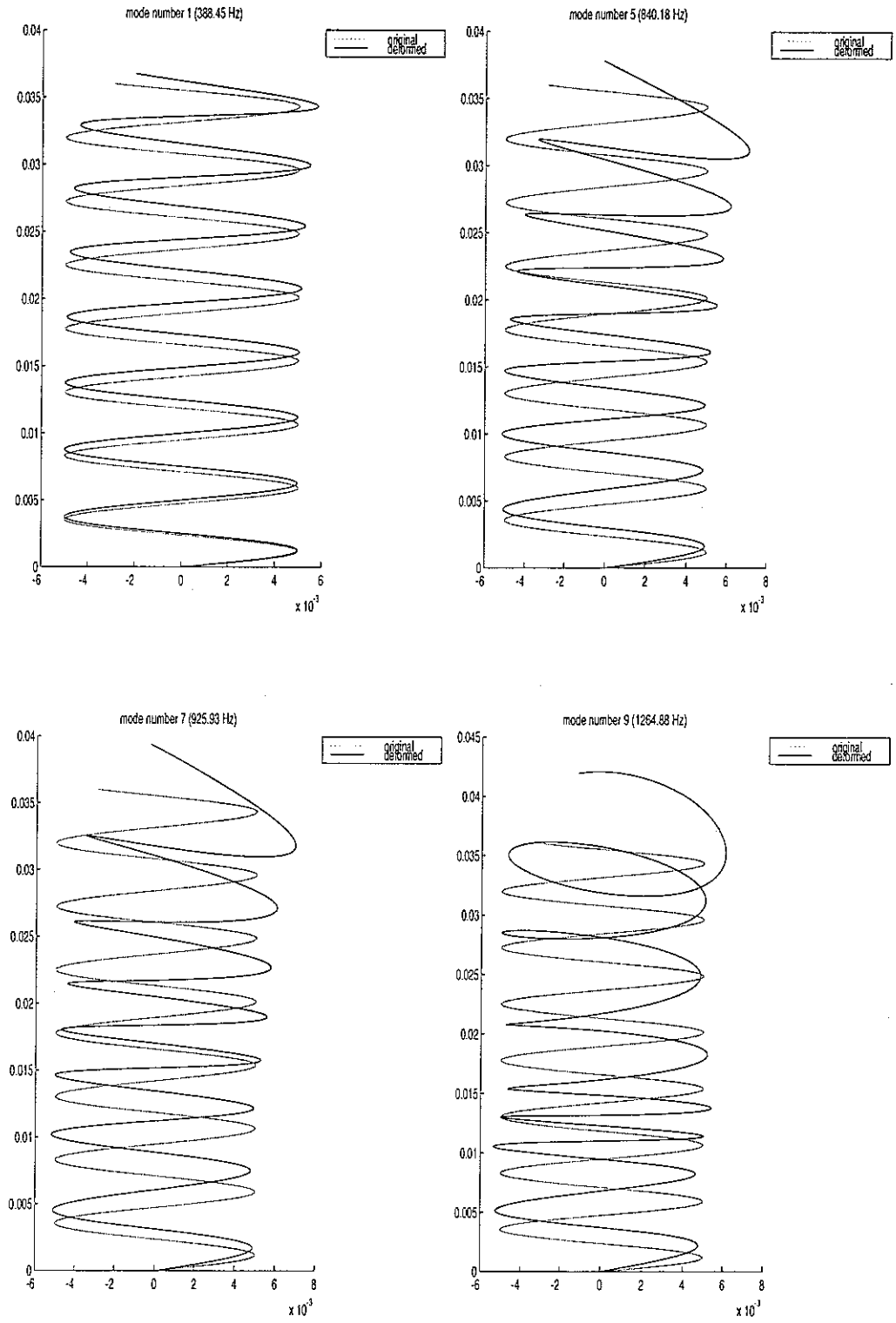

Fig. 4 Forced responses for spring 1 (axially loaded top end with clamped bottom end)

3.2. Transfer stiffness

The dynamic stiffness is an important parameter required in order to model vibration isolation. At a given frequency of excitation the ratio between force and displacement can be expressed as a complex stiffness. Transfer stiffness can be obtained from equation (34) by introducing a displacement vector at one end with only one component non-zero and calculating the blocked force in this direction at the other end. Fig. 5 and 6 show the axial and transverse transfer stiffness for spring 3 compared to the static stiffness. The axial transfer stiffness found in this method has a sharp dip at 16 Hz whereas the transverse transfer stiffness has a sharp dip at 11 Hz. Both transfer stiffnesses have a peak around 30 Hz. Above about 50 Hz, the transfer stiffness magnitudes increase with frequency except at resonances.

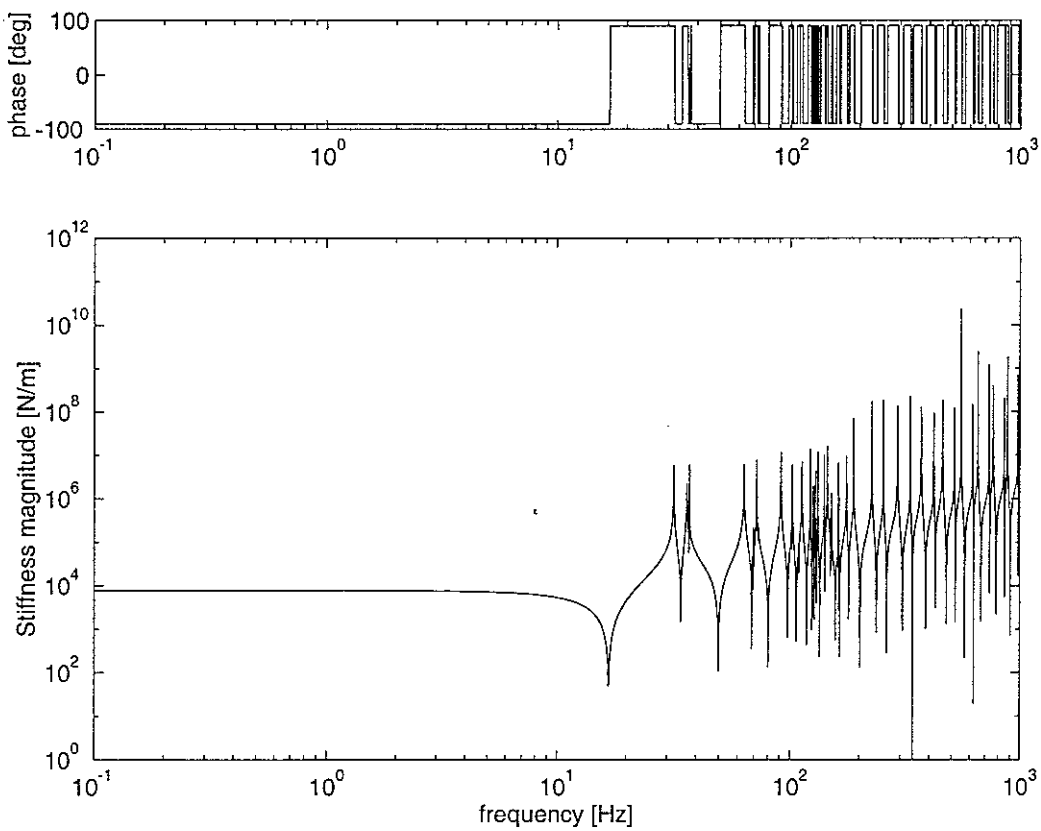

Fig. 5 Phase and Magnitude of axial transfer stiffness of spring 3

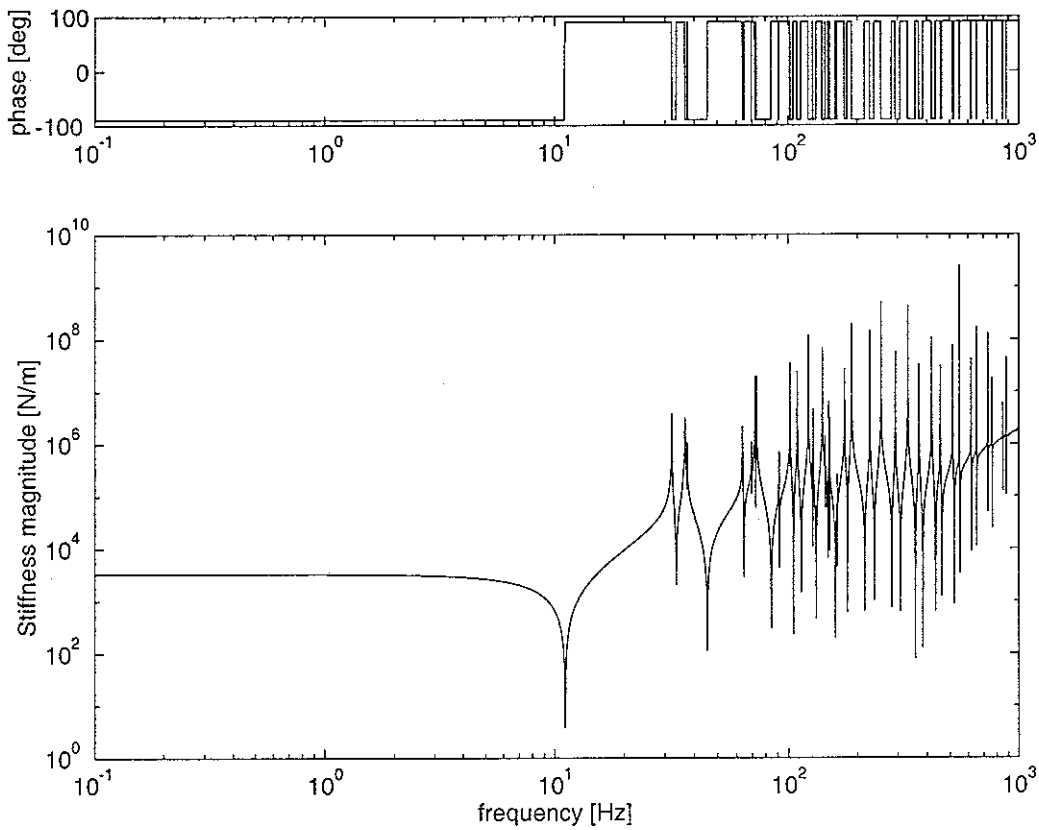

Fig. 6 Phase and Magnitude of transverse transfer stiffness of spring 3

3.3. Wave propagation

The dispersion curve, wave number versus frequency, gives a lot of information about the wave propagation. For a given frequency, ω, the harmonic equations of motion were solved to find the complex valued wave number, k from equation (20).

Fig. 7 shows the dispersion curves of each motion of a spring. It can be seen that there are three regimes separated by wave type. In the regime I, the lower frequency area less than point 4, travelling waves 1 and 2 start from zero wave number. These waves are extensional and torsional waves of the spring respectively. They have similar wave number and so couple easily. The near field waves of the wire 3 and 4 start with a wave length equal to the circumference of the spring divided by the cosine of helix angle. Wave 3 corresponds to the breathing motion of the coil which includes tension in the wire. Wave 4 relates to the bending moment about normal axis of the wire. Waves 5 and 6 correspond to shear waves of the wire. As the wave length of wave 1 approaches twice of circumference of the spring divided by the cosine of the helix angle, the predominant wave type changes from travelling wave to near field wave in the regime II, between point 2 and 1. Waves 4 and 5 diverge and change from

near field waves to travelling waves in this regime. In the regime III, above point 3, the travelling wave 1 changes to a near field wave, and wave 4 returns to a near field wave. In the cases of near field waves, the wave numbers have complex values which corresponds to a decay rate from the forcing point. In this high frequency regime there are only two travelling waves, 5 and 6.

The dispersion curves of the presented method for spring 3 are compared with Wittrick's approximate curves [4] in Fig. 8. Wittrick found the phase velocities and group velocities of a coil spring assuming that the helix angle is zero. For long wave length and small helix angle, the phase velocities are quite accurate for waves 1 and 2 (V and V' of equation 2 and 3). The other phase velocities are not acceptable in the frequency range of interest. The error comes from the approximate expression for the root of the cubic equation and other assumptions. The group velocities, the partial derivative of frequency with respect to wave number, are more important than phase velocities in describing energy propagation. These have complex values which corresponds to a decay rate from the forcing point. Except for wave 1 and wave 2 all group velocities go to zero in Wittrick's model as the square of the wave length tends to infinity. In this case the group velocities of waves 1 and 2 are the same as the phase velocities. This means that both waves transport their energies without dispersion but no energies related to other waves are transported at all. The graphical solutions of the presented method are not consistent with these group velocities for large wave numbers, indicating that dispersion does occur and that energy transport is shared among all waves.

From this it can be inferred that the energy of the spring is mainly transported by waves 1 and 2 at lower frequencies. Wave 5 carries the energy at higher frequencies.

3.4. The effect of helical angle on waves

As mentioned in the previous section, wave characteristics change at certain transition frequencies. Three non-material parameters, helix angle, helix radius and wire radius, affect these points. The helix angle can have a major effect, whilst the others have less influence [10]. In general, when the helix angle is greater than 15° the dispersion curves of a spring approach those of a straight beam. The variations of dispersion curves of each wave for spring 3 with helix angle from 0° to 15° are shown in Fig 9. If the transition points are interpolated, they can be seen to change by certain functions. Points 1 to 3 change by trigonometric functions and point 4 changes by a linear function. Fig. 10 is the plot of the

frequency variation of the transition frequencies with helix angle and compared with the interpolated functions. In this range point 2 is more sensitive than any other points to the helix angle. As the helix angle increases, point 2 approaches point 1. This means wave 4 has same dispersion characteristics as wave 5 below the frequency of the cross point. There are actually complex conjugate of one another.

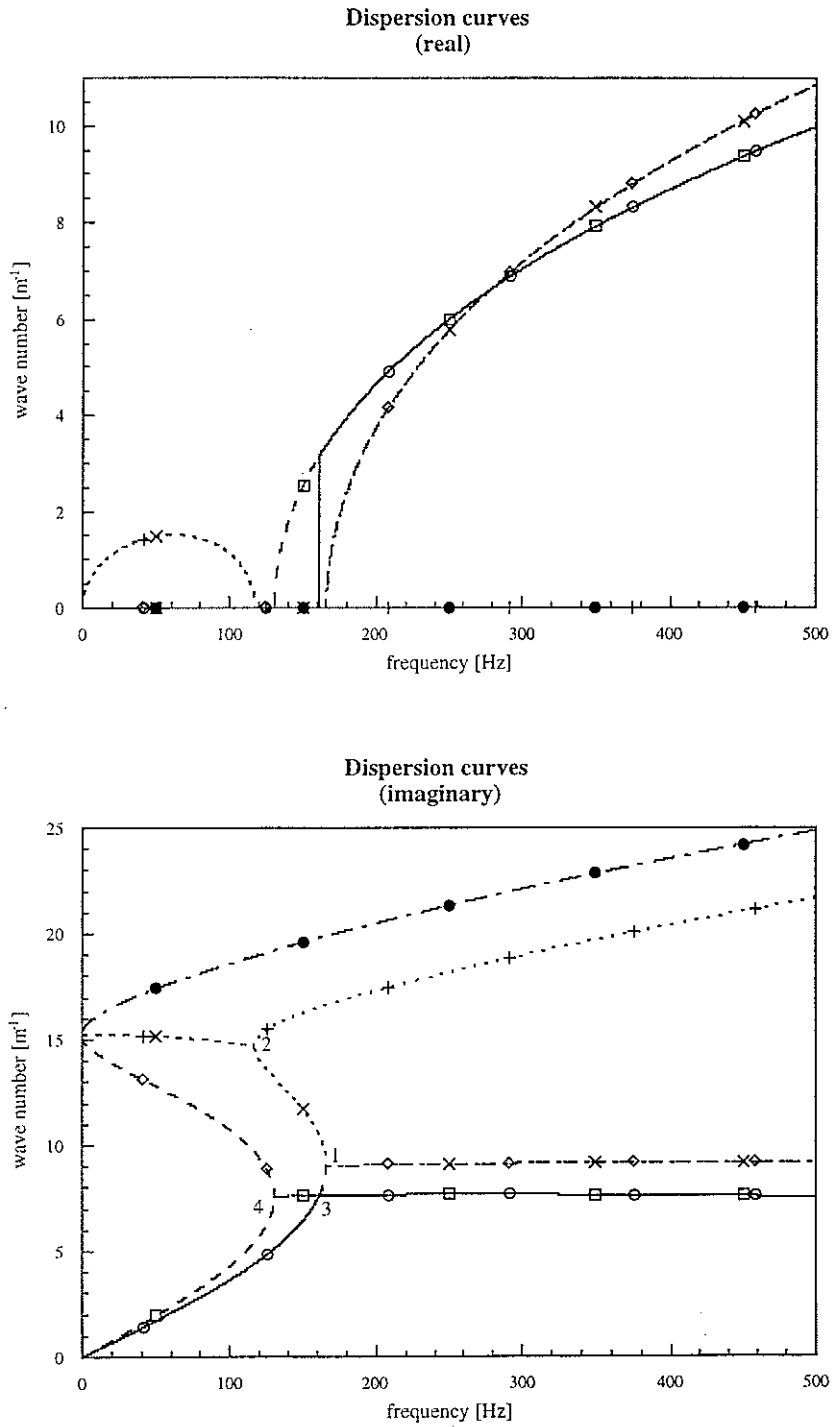

Fig. 7 Dispersion curves of the waves for spring 3 (o: wave 1, □: wave 2, ◊: wave 3, ×: wave 4, +: wave 5, ●: wave 6)

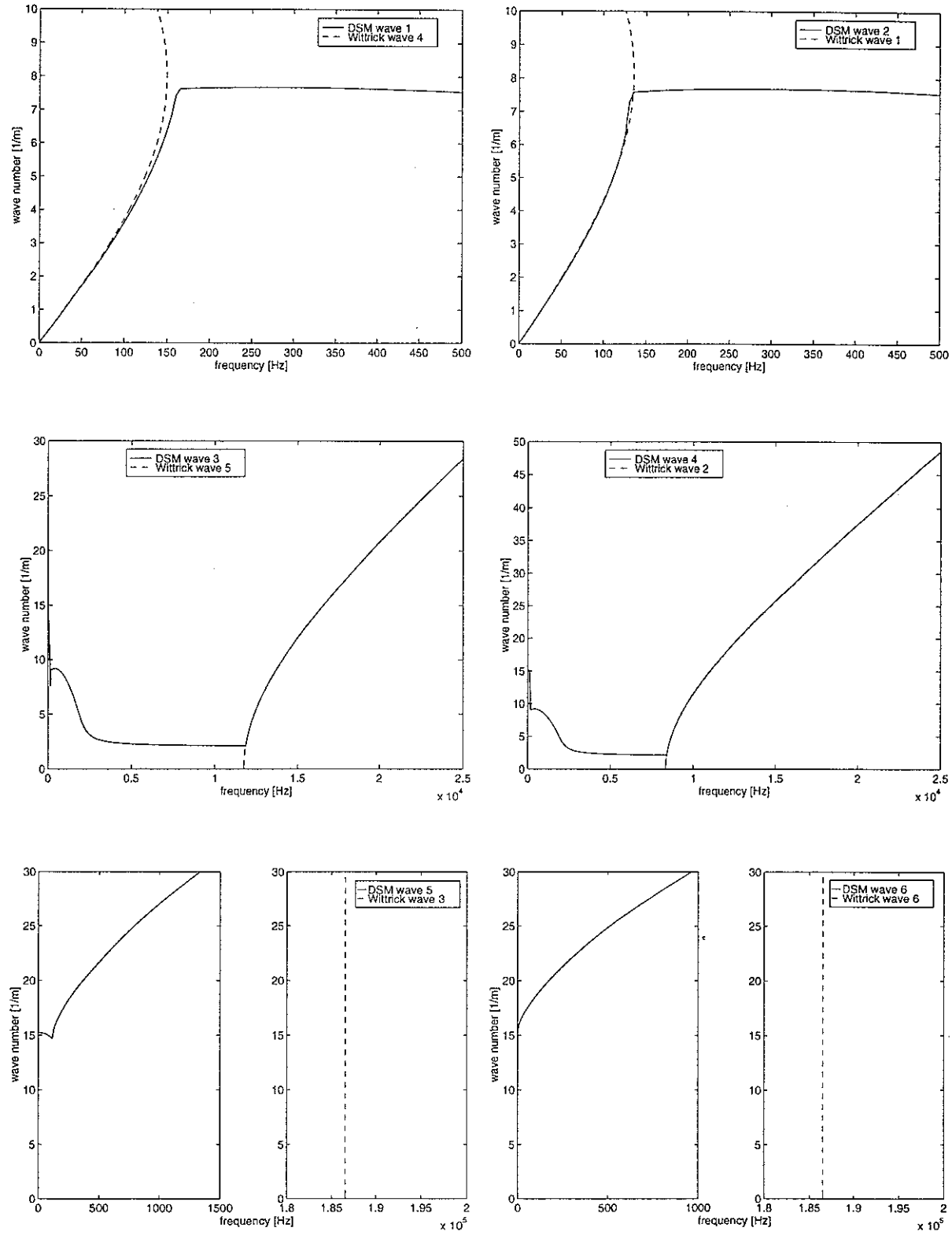

Fig. 8 Comparison of dispersion curves for spring 3 between the dynamic stiffness matrix method and ref. [4] (DSM: the wave obtained by dynamic stiffness matrix method, Wittrick: Wittrick's wave)

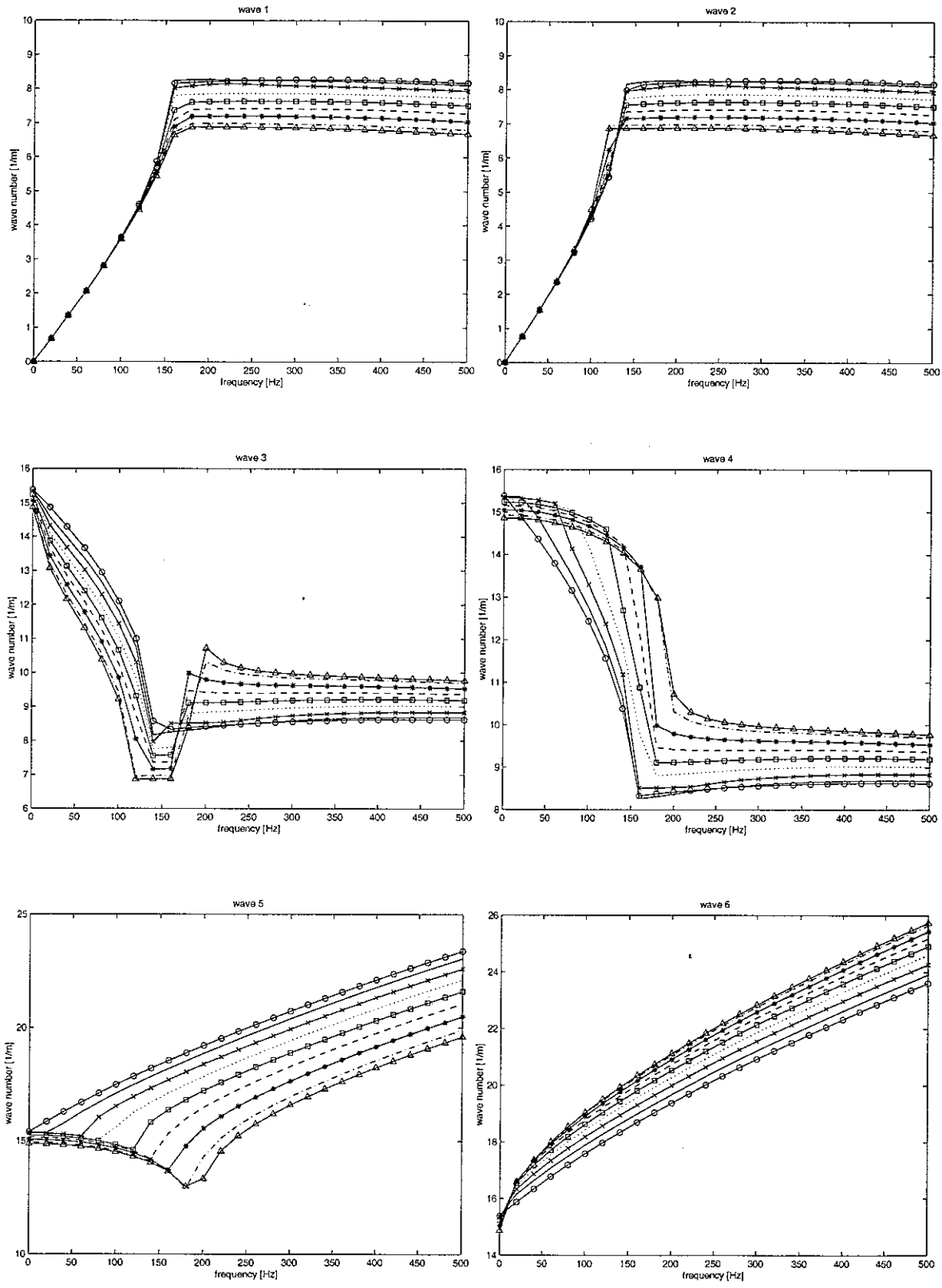

Fig. 9 Variation of dispersion curves of each wave for spring 3 with helix angle (o: α=0°, —: α=2°, ×: α=4°, ···: α=6°, □: α=8°, ----: α=10°, *: α=12°, -·-·: α=14°, Δ: α=15°)

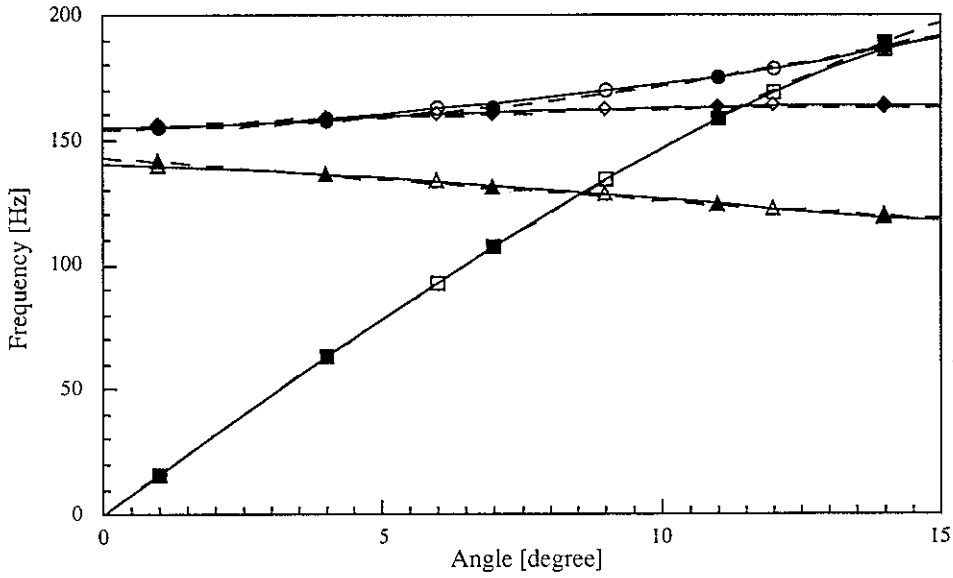

Fig. 10 Comparison of frequency variation with helix angle between calculated and estimated (o:calculated point 1, ●: $f = -120 \times \cos 3.1\alpha + 274.5$, □:calculated point 2, ■: $f = 228 \times \sin 4\alpha$, ◊:calculated point 3, ◆: $f = 8.5 \times \sin 6\alpha + 154.7$, Δ:calculated point 4, ▲: $f = -97.5\alpha + 143$)

4. CONCLUSIONS

Based on Timoshenko beam theory and Frenet formula, the dynamic stiffness matrix for a helical spring has been derived. The natural frequencies were calculated by using the dynamic stiffness method. The results computed by the presented method were compared with various published methods and experimental results and were in good agreement. The response for the forced vibration has been determined. Also the axial and transverse transfer stiffnesses for spring 3 have been computed and compared to the static stiffness, to show the high frequency behaviour. Investigation of the dispersion curves led to infer the wave travel in a helical spring and to explain the coupling effect.

The dispersion curves which are compared with ref. [4] illustrate the wave propagation. They show the predominant wave type and energy transportation in different frequency ranges. Also, the effect of helix angle on the wave characteristics is investigated.

The advantages of the presented method are to calculate natural frequencies and displacement vector in a range of frequencies chosen by user. Compared with the transfer matrix method, the run time is very short and responses can be obtained easily for a forced vibration analysis. In contrast with the finite element method, no geometrical modelling is necessary.

REFERENCES

1. A. E. M. Love, The propagation waves of elastic displacement along a helical wire. *Trans. Camb. Phil. Soc.*, (1900).

2. S. P. Timonshenko, *Theory of elastic stability*, 1st Edn., McGraw Hill, New York & London (1936).

3. A. M. Wahl, *Mechanical springs*, 2nd Edn., McGraw Hill, New York, (1963).

4. W. H. Wittrick, On elastic wave propagation in helical springs. *Int. J. Mech. Sci.* **8**, 25 (1966).

5. W. Jiang, W. Jones, K. Wu and T. Wang, Non-linear and linear, static, and dynamic analyses of helical springs. *Proc. of the 30th AIAA/ASME/ASCE/AHS/ASC Structures, Structural Dynamics and Materials Conference, Mobile, Ala., Apr.*, 386 (1989).

6. W. Jiang, W. K. Jones, T. L. Wang and K. H. Wu, Free vibration of helical springs. *Trans. ASME* **58**, 222 (1991).

7. Sunil K. Sinha and George A. Costello, The numerical solution of the dynamic response of helical springs. *Int. J. Num. Meth. Engng.* **12**, 949 (1978).

8. Jaehyung Lee, Hong Hee Yoo and Jang Moo Lee, High frequency characteristics of a front wheel suspension, *Vehicle System Dynamics* **28**, Oct. 261, (1997).

9. John E. Mottershead, Finite elements for dynamical analysis of helical rods. *Int. J. Mech. Sci.* **22**, 267 (1980).

10. D. Pearson, The transfer matrix method for the vibration of compressed helical springs. *J. Mech. Engng Sci.* **24**, 163 (1982).

11. Vebil Yildirim, Investigation of parameters affecting free vibration frequency of helical springs. *Int. J. Num. Meth. Engng.* **39**, 99 (1996).

12. V. Yildirim and N. Ince, Natural frequencies of helical springs of arbitrary shape. *J. Sound Vibration* **204** (2), 311 (1997).

13. Vebil Yildirim, An efficient numerical method for predicting the natural frequencies of cylindrical helical springs. *Int. J. Mech. Sci.* **41**, 919 (1999).

14. D. Pearson and W. H. Wittrick, An exact solution for the vibration of helical springs using a Bernoulli-Euler model. *Int. J. Mech. Sci.* **28**, 83 (1986).

15. E. Kreyszig, *Advanced Engineering Mathematics*, 3rd Edn., Wiley, New York (1972).

16. G. B. Warburton, *The dynamical behaviour of structures*, 2nd Edn., Pergamon Press Ltd., Oxford (1976).

Appendix A. The submatrices $\mathbf{S}_{ij}$ and $\mathbf{T}_{ij}$ for a helical spring

$$\mathbf{S}_{11}=\begin{bmatrix} 0 & \tau & -\kappa & 0 & 1 & 0 \\ -\tau & 0 & 0 & -1 & 0 & 0 \\ \kappa & 0 & 0 & 0 & 0 & 0 \\ 0 & 0 & 0 & 0 & \tau & -\kappa \\ 0 & 0 & 0 & -\tau & 0 & 0 \\ 0 & 0 & 0 & \kappa & 0 & 0 \end{bmatrix},\quad \mathbf{S}_{12}=\begin{bmatrix} \frac{1}{GA\gamma} & 0 & 0 & 0 & 0 & 0 \\ 0 & \frac{1}{GA\gamma} & 0 & 0 & 0 & 0 \\ 0 & 0 & \frac{1}{EA} & 0 & 0 & 0 \\ 0 & 0 & 0 & \frac{1}{EI_u} & 0 & 0 \\ 0 & 0 & 0 & 0 & \frac{1}{EI_v} & 0 \\ 0 & 0 & 0 & 0 & 0 & \frac{1}{GI_w} \end{bmatrix}$$

$$\mathbf{S}_{22}=\begin{bmatrix} 0 & \tau & -\kappa & 0 & 0 & 0 \\ -\tau & 0 & 0 & 0 & 0 & 0 \\ \kappa & 0 & 0 & 0 & 0 & 0 \\ 0 & 1 & 0 & 0 & \tau & -\kappa \\ -1 & 0 & 0 & -\tau & 0 & 0 \\ 0 & 0 & 0 & \kappa & 0 & 0 \end{bmatrix},\quad \mathbf{T}_{21}=\begin{bmatrix} \rho A & 0 & 0 & 0 & 0 & 0 \\ 0 & \rho A & 0 & 0 & 0 & 0 \\ 0 & 0 & \rho A & 0 & 0 & 0 \\ 0 & 0 & 0 & \rho I_u & 0 & 0 \\ 0 & 0 & 0 & 0 & \rho I_v & 0 \\ 0 & 0 & 0 & 0 & 0 & \rho I_w \end{bmatrix}$$

Appendix B. Modeshapes of spring 1 by NASTRAN

Following modeshapes of spring 1 with both ends clamped are obtained by NASTRAN

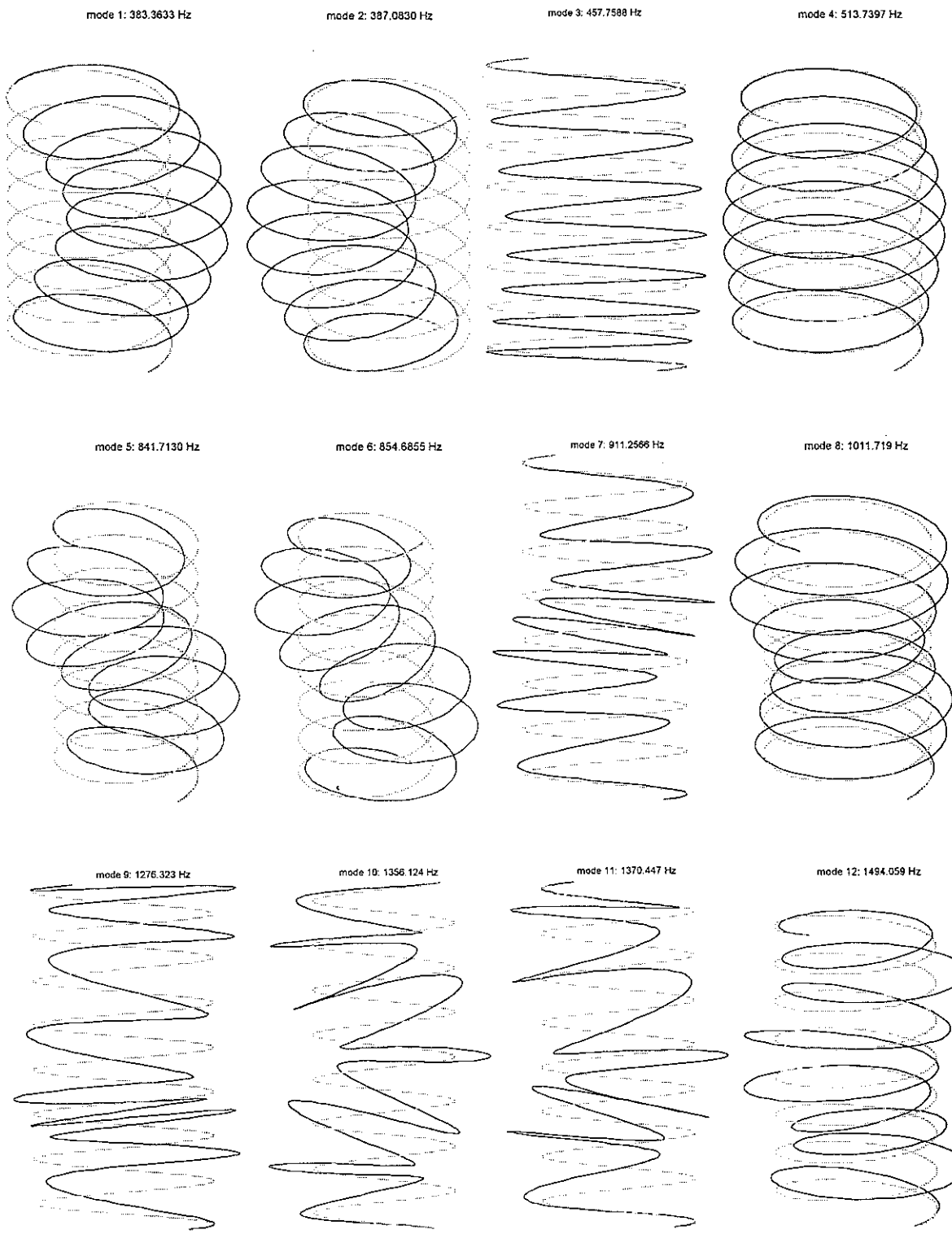

mode 13: 1639.530 Hz

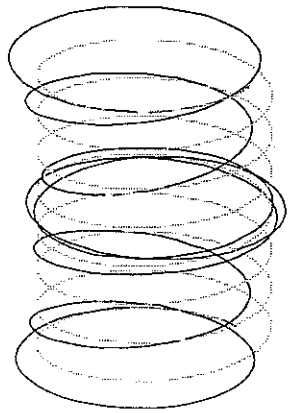

mode 14: 1768.476 Hz

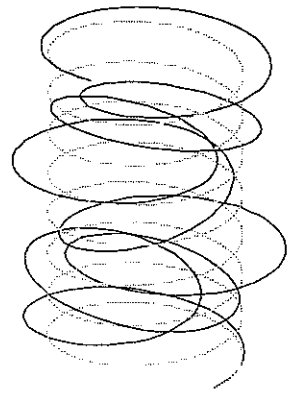

mode 15: 1811.345 Hz

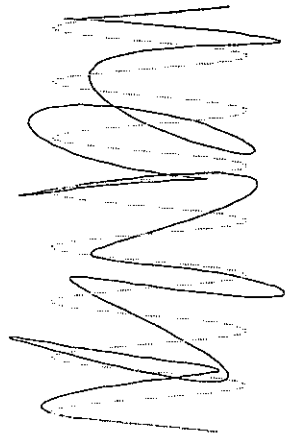

mode 16: 1921.436 Hz

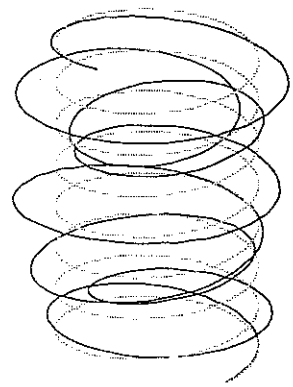

mode 17: 1943.213 Hz

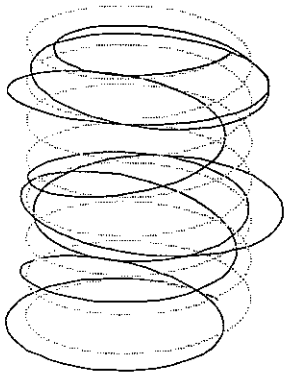

mode 18: 2087.872 Hz

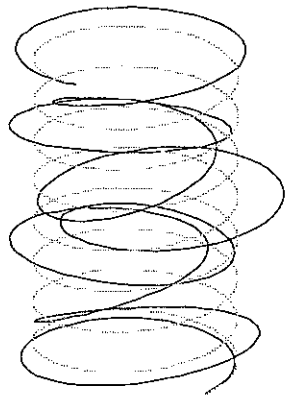

mode 19: 2099.948 Hz

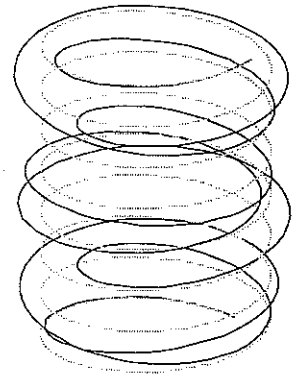

mode 20: 2201.797 Hz

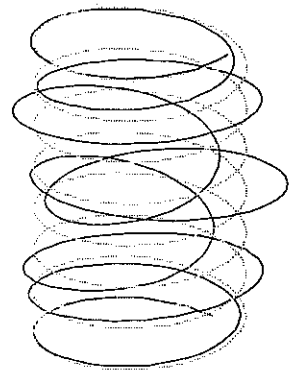

mode 21: 2218.310 Hz

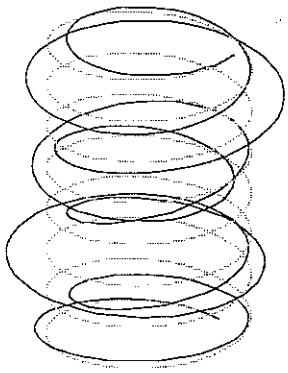

mode 22: 2243.560 Hz

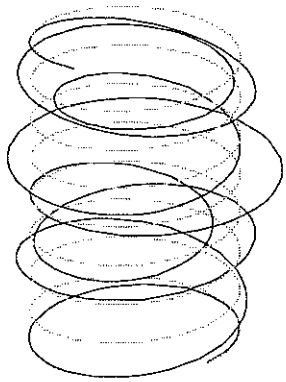

mode 23: 2365.933 Hz

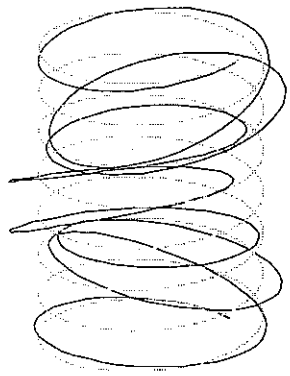

mode 24: 2370.624 Hz

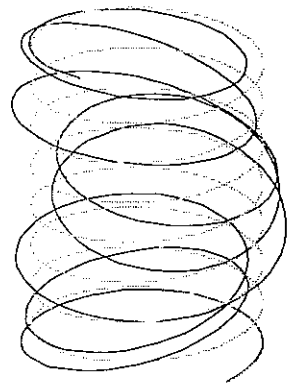

mode 25: 2402.309 Hz

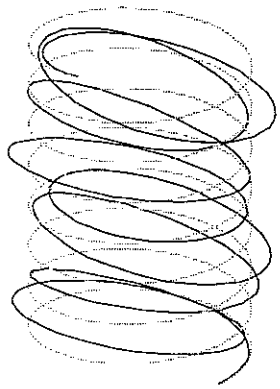

mode 26: 2534.693 Hz

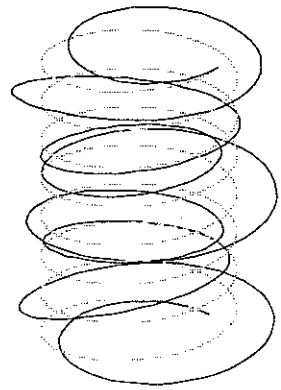

mode 27: 2655.004 Hz

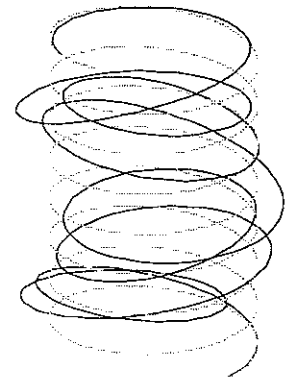

mode 28: 2674.472 Hz

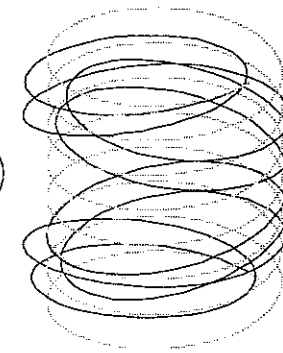

mode 29: 2758.234 Hz

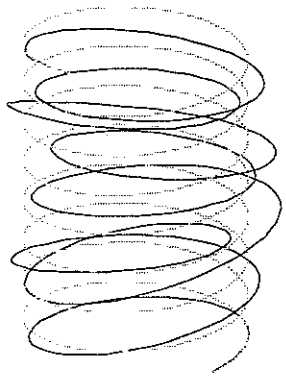

mode 30: 2849.079 Hz

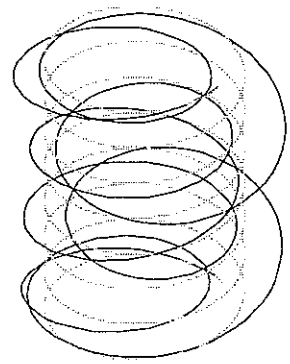

mode 31: 2856.856 Hz

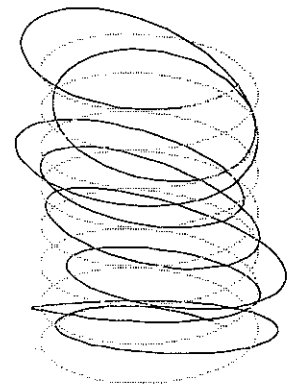

mode 32: 2928.097 Hz

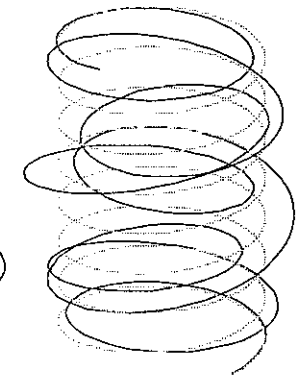

mode 33: 2929.115 Hz

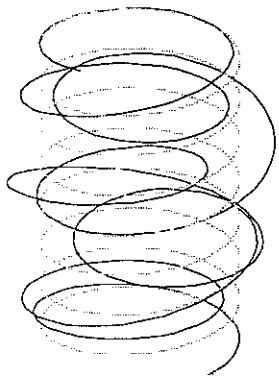

mode 34: 3274.935 Hz

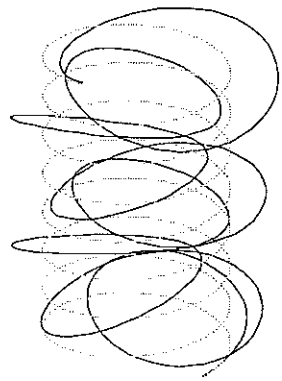

mode 35: 3450.310 Hz

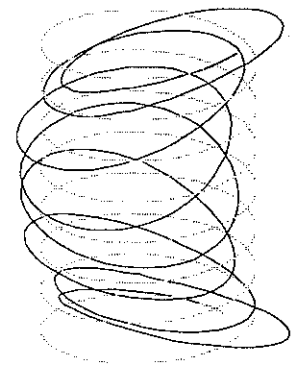

mode 36: 4095.136 Hz

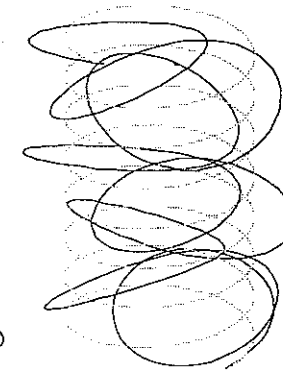

APPENDIX C. Program code for MATLAB

The MATLAB program is composed of main program "CSPRING.m" and function program "DEXP.m".

CSPRING.m

```
% Program for dynamic analysis of a coil spring
%             Programmed by
%    Jaehyung Lee and D.J.Thompson
%              1. Aug 1999
%                Ver 2.0
%
clear all; clc;
format long e;
%
t=cputime;
% variables
r = input('wire radius [m]?: ');
R = input('helix radius [m]?: ');
alpha = input('helix angle [degree]?: ');
n = input('number of turns?: ');
E = input('Young"s modulus [N/m^2]?: ');
nu = input('Poisson"s ratio?: ');
rho = input('density [kg/m^3]?: ');
P = input('preload [Kg]?: ');
fi = input('initial frequency [Hz]?: ');
fo = input('final frequency [Hz]?: ');
fr = input('frequency resolution [Hz]?: ');
bc = input('boundary conditions? free-free=1, clamped-free=2, pivot-pivot=3: ');
%
D2R = pi/180;                          % conversion factor from degree to radian
alpha = alpha.*D2R;
h = 2*pi*R*n*tan(alpha);               % height of the coil spring
area = pi.*r.^2;                       % c/s area
G = E./(2.*(1+nu));                    % shear modulus
mu = rho*area;                         % mass per unit length
s = (2*pi*R*n)/cos(alpha);             % length measured according to wire
%
I = area.*r^2/4;                       % 2nd moment of area about the wire axis
kappa = cos(alpha)^2/R;                % the curvature
tau = sin(alpha)*cos(alpha)/R;         % the torosity
gamma=6*(1+nu)^2/(7+12*nu+4*nu^2);     % shear factor
% rotation matrix
   p0=0;
   pl=2*n*pi;
   Q0=[0 -cos(p0) -sin(p0);
       cos(alpha) sin(alpha)*sin(p0) -sin(alpha)*cos(p0);
       sin(alpha) -cos(alpha)*sin(p0) cos(alpha)*cos(p0)];
   Ql=[0 -cos(pl) -sin(pl);
       cos(alpha) sin(alpha)*sin(pl) -sin(alpha)*cos(pl);
       sin(alpha) -cos(alpha)*sin(pl) cos(alpha)*cos(pl)];
   RT=zeros(12);
   RT(1:3,1:3)=Q0;
   RT(4:6,4:6)=Q0;
   RT(7:9,7:9)=Ql;
   RT(10:12,10:12)=Ql;
%
b=[1/(G*area*gamma), 1/(E*area), 1/(E*I), 1/(2*G*I)]';
% stiffness matrix
k(1,1) = 1/b(1);
k(1,8) = -tau/b(1);
k(1,9) = kappa/b(1);
k(1,11) = -1/b(1);
k(2,2) = 1/b(1);
k(2,7) = tau/b(1);
k(2,10) = 1/b(1);
```

```
k(3,3) = 1/b(2);
k(3,7) = -kappa/b(2);
k(4,4) = 1/b(3);
k(4,11) = -tau/b(3);
k(4,12) = kappa/b(3);
k(5,5) = 1/b(3);
k(5,10) = tau/b(3);
k(6,6) = 1/b(4);
k(6,10) = -kappa/b(4);
% system matrix
A = zeros(12);
A(1,2) = tau;
A(1,3) = -kappa;
A(1,5) = 1;
A(1,7) = b(1);
A(2,1) = -tau;
A(2,4) = -1;
A(2,8) = A(1,7);
A(3,1) = kappa;
A(3,9) = b(2);
A(4,5) = tau;
A(4,6) = -kappa;
A(4,10) = b(3);
A(5,4) = -tau;
A(5,11) = A(4,10);
A(6,4) = kappa;
A(6,12) = b(4);
A(7,8) = tau;
A(7,9) = -kappa;
A(7,11) = P*sin(alpha)/(E*I);
A(7,12) = -P*cos(alpha)/(2*G*I);
A(8,7) = -tau;
A(8,10) = -P*cos(alpha)/(E*I);
A(9,7) = kappa;
A(9,10) = P*cos(alpha)/(E*I);
A(10,8) = 1;
A(10,11) = tau+P*R*cos(alpha)/(E*I);
A(10,12) = -kappa+P*R*sin(alpha)/(2*G*I);
A(11,7) = -1;
A(11,10) = -tau-P*R*cos(alpha)/(E*I);
A(12,10) = kappa-P*R*sin(alpha)/(E*I);
%
fall = [fi:fr:fo]';
nf = length(fall);
lam = zeros(nf,12);
for in=1:nf;
    f = fall(in);
    A(7,1) = -(2*pi*f)^2*mu;
    A(8,2) = A(7,1);
    A(9,3) = A(7,1);
    A(10,4) = -(2*pi*f)^2*rho*I-P*sin(alpha);
    A(11,5) = A(10,4);
    A(12,6) = 2*(-(2*pi*f)^2*rho*I)+P*cos(alpha);
% find wave number vs. freqency
    [V,ev] = eig(A);
    lamthis = diag(ev).';
    [dum,iii] = sort(imag(lamthis));
    lamthis = lamthis(iii);
    for iii=1:11
       ib=[iii iii+1];
       if abs(imag(lamthis(iii+1))-imag(lamthis(iii)))<1e-10
          [dum,it] = sort(real(lamthis(ib)));
          lamthis(ib) = lamthis(ib(it));
       end
    end
    lam(in,:) = lamthis;
%
    phi = V(1:6,:);
% Dynamic stiffness matrix
    [D1, DD1] = dexp(k, phi, ev, 0);
    [D2, DD2] = dexp(k, phi, ev, s);
    KD1 = [D1;D2];
    KD2 = [DD1; -DD2];
    kf = RT*KD2*inv(KD1)*inv(RT);
```

```
% Apply boundary condition
    if bc == 1
       ckf = kf;
    elseif bc ==2
       ckf = kf(7:12, 7:12);
    else
       ckf(1:3,1:3) = kf(4:6,4:6);
       ckf(4:6,4:6) = kf(10:12,10:12);
    end
% Find displacemet/force
    dkf(in) = det(inv(ckf));
    psi(in)=angle(dkf(in))/D2R;
% Phase angle
    if psi(in) < 1 & psi(in) > -1
       psi(in)=90;
    else
       psi(in)=-90;
    end
end
clf
% Plot 'displacement/force'
figure(1)
axes('position',[0.1, 0.75, 0.8,0.15]);
grid
plot(fall, psi, 'b')
ylabel('phase [deg]');
axes('position',[0.1, 0.1, 0.8,0.6]);
semilogy(fall, abs(dkf), 'b')
xlabel('Frequency [Hz]');
ylabel('Displacement/Force [m/N]')
grid
% plot 'Dispersion curve'
figure(2)
subplot(211)
plot(fall, [abs(real(lam(:,7))), abs(real(lam(:,8))), abs(real(lam(:,9))),...
     abs(real(lam(:,10))), abs(real(lam(:,11))), abs(real(lam(:,12)))])
title('real')
ylabel('wave number [1/m]')
subplot(212)
plot(fall, [imag(lam(:,7)), imag(lam(:,8)), imag(lam(:,9)), imag(lam(:,10)),...
     imag(lam(:,11)), imag(lam(:,12))])
title('imaginary')
xlabel('frequency [Hz]')
ylabel('wave number [1/m]')
%
run_time=cputime-t
```

DEXP.m

```
function [D1, DL]=dexp(s, phi, ev, fhi)
dis = fhi.*diag(ev);
dx = exp(dis.');
d1x = dx*ev;
d2x = dx*ev.^2;
d3x = dx*ev.^3;
D1 = phi*diag(dx);
D2 = phi*diag(d1x);
D3 = phi*diag(d2x);
D4 = phi*diag(d3x);
DD = [D2;D1];
[n, m]=size(s);
td = zeros(n,12);
for ii = 1:n
   for jj = 1:m
      td(ii,:) =td(ii,:)+s(ii,jj).*DD(jj,:);
   end
end
%
DL = [td(1,:); td(2,:); td(3,:); -td(4,:); -td(5,:); td(6,:)];
```